THE JOURNAL OF PHYSICAL CHEMISTRY Letters

Letter

pubs.acs.org/JPCL

Intrinsic Material Properties Dictating Oxygen Vacancy Formation Energetics in Metal Oxides

Ann M. Deml,[†,‡] Aaron M. Holder,[§,∥] Ryan P. O'Hayre,[†] Charles B. Musgrave,[§] and Vladan Stevanović*[,†,‡]

[†]Colorado School of Mines, Golden, Colorado 80401, United States

[‡]National Renewable Energy Laboratory, Golden, Colorado 80401, United States

[§]University of Colorado—Boulder, Boulder, Colorado 80309, United States

Supporting Information

ABSTRACT: Oxygen vacancies (V_O) in oxides are extensively used to manipulate vital material properties. Although methods to predict defect formation energies have advanced significantly, an understanding of the intrinsic material properties that govern defect energetics lags. We use first-principles calculations to study the connection between intrinsic (bulk) material properties and the energy to form a single, charge neutral oxygen vacancy (E_V). We investigate 45 binary and ternary oxides and find that a simple model which combines (i) the oxide enthalpy of formation (ΔH_f), (ii) the midgap energy relative to the O 2p band center ($E_{O\,2p}$ + $(1/2)E_g$), and (iii) atomic electronegativities reproduces calculated E_V within ∼0.2 eV. This result provides both valuable insights into the key properties influencing E_V and a direct method to predict E_V. We then predict the E_V of ∼1800 oxides and validate the predictive nature of our approach against direct defect calculations for a subset of 18 randomly selected materials.

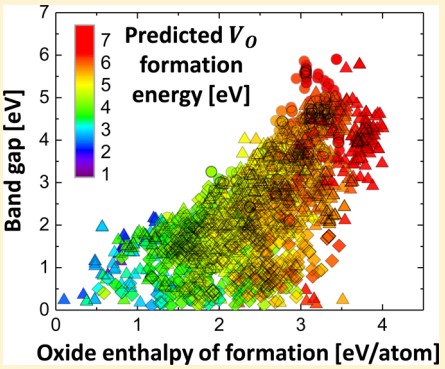

The energy to form oxygen vacancies V_O largely dictates oxygen off-stoichiometry and, thus, is a key quantity influencing material behaviors such as electronic and ionic conductivity, catalytic activity, and optical properties that are used in applications such as transparent conductors,[1] solid oxide fuel cells,[2,3] solar thermochemical fuel cycles,[4,5] electrochemical supercapacitors,[6] sensors,[7] catalytic membrane reactors,[8] thermal barrier coatings,[9] and refractories.[10] Modern first-principles calculations have become significantly more accurate in predicting the point defect formation energies of individual systems.[11−13] Simultaneously, high throughput approaches have produced large computational databases of perfect (defect-free) materials.[14−16] Nevertheless, rapid predictions of the properties of defective systems remain a challenge largely due to prohibitive computational costs. As a result, understanding of the detailed effects of chemical bonding and crystal structure on defect energies, as is critical for understanding the behaviors of "real" materials, is still relatively rudimentary and limited to individual cases. Similarly, our ability to understand and predict chemical trends across large chemical spaces when screening for target defect energies remains limited.

Herein, we demonstrate an approach to move beyond high throughput calculations of perfect materials to rapid predictions of defect systems, a key for enabling materials genome inspired design and discovery of materials. We use first-principles defect calculations to investigate the intrinsic properties of oxides that govern neutral oxygen vacancy formation energies E_V. We investigate 45 main group and transition metal (TM) oxides covering a range of compositions and crystal structures. After examining an extensive list of bulk material properties and constituent elemental properties, we find that a linear combination of three terms reproduces calculated E_V within ∼0.2 eV (Figure 1a). The achieved accuracy is similar to differences in E_V calculated by different computational methods[12] and approaches that of experiment.[17,18] Thus, E_V can be accurately predicted from basic properties that collectively describe the strength and character of chemical bonding and the effective electronic energy to transfer the "oxygen vacancy electrons" from the O 2p band into the newly created V_O defect levels.

In addition, our model enables the prediction of E_V from simple calculations of bulk materials, which allows for the use of material properties from existing databases while avoiding demanding supercell calculations. This is particularly advantageous when studying trends across large chemical spaces or when searching for and classifying materials based on E_V. To validate the predictive power of our E_V model, we used the National Renewable Energy Laboratory's computational materials database (NRELMatDB)[14] to predict E_V for ∼1800 oxides. The performance of our model was validated against direct E_V calculations for a subset of 18 (1%) randomly chosen

Received: April 6, 2015
Accepted: May 6, 2015

DOI: 10.1021/acs.jpclett.5b00710
J. Phys. Chem. Lett. 2015, 6, 1948−1953

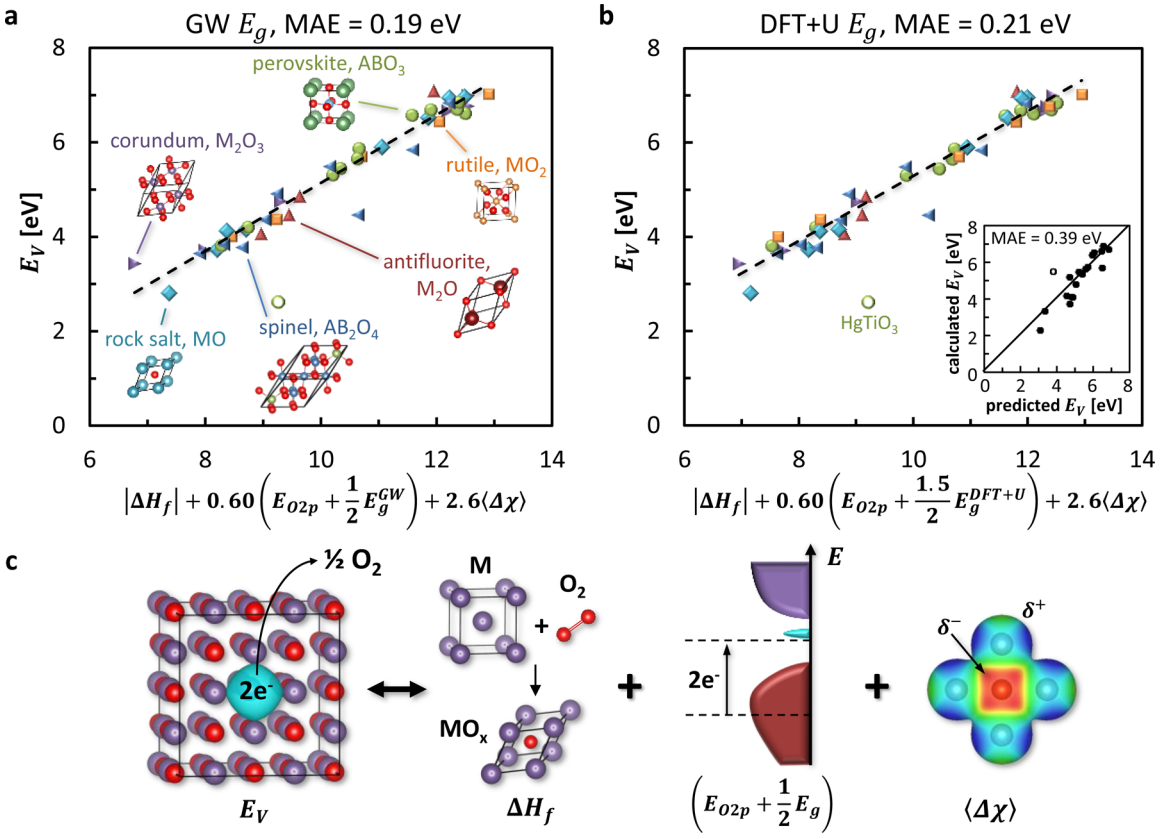

Figure 1. The formation energy of a neutral oxygen vacancy (E_V) can be accurately modeled by a linear combination of (i) the oxide enthalpy of formation (ΔH_f), (ii) the midgap energy relative to the O 2p band center ($E_{O\ 2p} + (1/2)E_g$), and (iii) atomic electronegativities ($\langle\Delta\chi\rangle$). Models with band gap values from both GW (a) and DFT+U (b) calculations reproduce calculated E_V values with a mean absolute error (MAE) of ~0.2 eV; DFT +U calculations provide a significant decrease in computational cost. In the inset of (b), direct E_V calculations of 18 oxides not included in the model development yield a MAE of 0.39 eV and provide an assessment of the predictive accuracy of our E_V model. Open symbols indicate observed outliers as discussed in the text. (c) Individual contributions to the E_V model describe (i) the strength of the metal−oxygen bonds (ΔH_f), (ii) the energy needed to transfer the electrons left behind by the removed neutral O atom ($E_{O\ 2p} + (1/2)E_g$), and (iii) the charge transfer between chemically bonded O and metal atoms ($\langle\Delta\chi\rangle$).

oxides, including complex ternary and quaternary chemistries, resulting in a mean absolute error (MAE) of 0.39 eV.

Previous studies of oxygen vacancy formation energetics have focused on rather limited variations in composition and structure and have reported E_V to be approximately correlated to the band gap energy (E_g)[19,20] or the oxide ΔH_f.[21] Although structure dependences have been suggested, no corresponding models or material descriptors have been provided. The E_V of certain perovskites have been correlated to the valence band maximum relative to the O 2p band center or to the Fermi energy.[22,23]

To analyze the relationships between E_V and bulk material properties, we directly compute the E_V of 45 oxides using the first-principles methods described below and in the Supporting Information. These oxides include both binary (one cation type) and ternary systems (two cation types) composed of main group and transition metals in antifluorite, corundum, rock salt, rutile, perovskite, and spinel crystal structures (Supporting Information Table S1). All reported E_V correspond to standard state conditions. Our previous work[24] showed that the E_V of a limited group of 10 perovskites can be accurately described with a linear combination of ΔH_f and E_g. Not surprisingly, the direct application of this result to the diverse set of 45 oxides computed here does not perform well, as shown in Supporting Information Figure S1. The performance of our previous model is satisfactory only within a single crystal structure group, implying that the coefficients in the linear combination must be determined separately for every crystal structure. Therefore, an important result of the present work is the "collapse" of the linear dependencies of different crystal structures into a single functional form.

As candidate descriptors, we include both bulk material properties available from calculations or directly from the crystal structure data (ΔH_f, E_g, O 2p band centers, Bader charges, atomic coordinations, bond lengths, etc.) as well as quantities characterizing the elemental constituents (Pauling electronegativities, Shannon ionic radii, etc.). A full list and description of the 13 candidate descriptors is provided in the Supporting Information.

As shown in Figure 1a, our analysis of the relationship between calculated E_V and these candidate basis descriptors reveals a relatively simple functional form for modeling E_V

$$E_V = 0.72\left[|\Delta H_f| + 0.60\left(E_{O\,2p} + \frac{1}{2}E_g^{GW}\right) + 2.6\langle\Delta\chi\rangle\right] - 2.07 \quad (1)$$

where ΔH_f is the oxide enthalpy of formation in eV/atom, $E_{O\ 2p}$ is the energy difference between of the valence band maximum and the center of the O 2p band in eV, E_g^{GW} is the calculated GW gap in eV, and $\langle\Delta\chi\rangle$ is the unitless average Pauling

DOI: 10.1021/acs.jpclett.5b00710
J. Phys. Chem. Lett. 2015, 6, 1948−1953

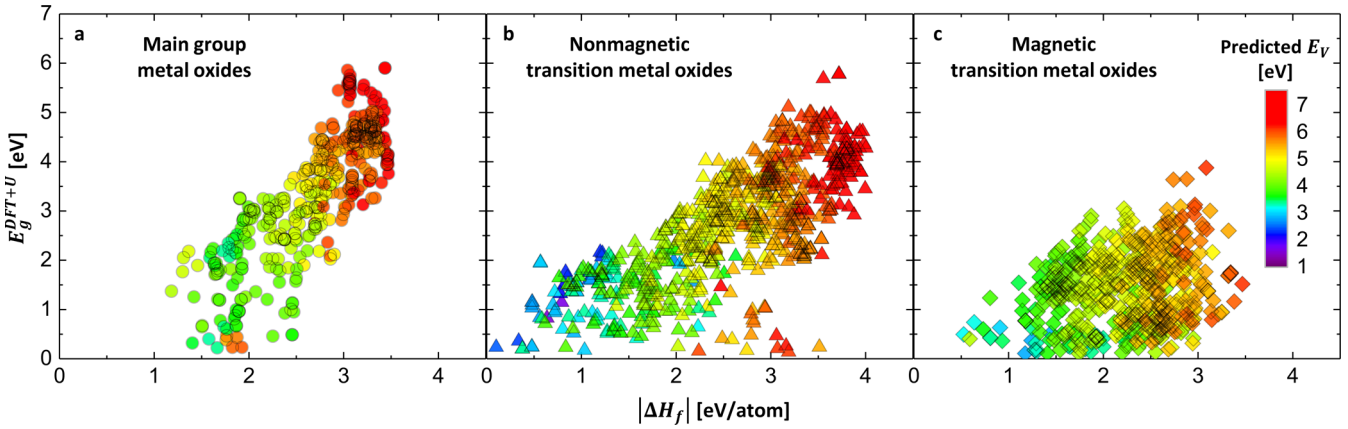

Figure 2. Predicted oxygen vacancy formation energies (E_V) for ~1800 oxide materials grouped according to those containing (a) only main group metals, (b) nonmagnetic transition metals, and (c) magnetic transition metals. Variations in the predicted E_V result primarily from the most dominant terms in the E_V model: the oxide enthalpy of formation (ΔH_f) and the band gap (E_g).

electronegativity difference between O atoms and the atoms forming their first coordination shell. Numerical values are provided in Supporting Information Table S1. The MAE of the model relative to the DFT+U calculated E_V is 0.19 eV. This accuracy is similar to differences in E_V calculated by different computational methods.[12]

Each quantity on the right-hand side of eq 1 could intuitively be expected to have some connection to E_V. However, it is considerably more difficult to predict that this particular linear combination of descriptors accurately describes E_V. Within the achieved accuracy, this set of quantities represents a *complete* set of descriptors. However, given the fact that all four quantities in eq 1 depend on both composition and crystal structure, this is not a set of mutually independent descriptors, and therefore, our model is not unique. Instead, our model is a reflection of the deeper dependence of E_V on material properties ultimately described by quantum mechanics. Within the considered set of basis descriptors, the four quantities in our model form a *minimal* set. Exclusion of any one of these quantities decreases the model accuracy as shown in Supporting Information Figures S1 and S2.

The physical picture that emerges from eq 1 (Figure 1c) indicates a dependence of E_V on the strength of the metal−oxygen bonds relative to the strength of bonding in pure elements, as described by the oxide ΔH_f. At the extreme, one can consider the formation (decomposition) of an oxide, and therefore ΔH_f, to be analogous to extensive filling (formation) of V_O in a metal (oxide). Therefore, it is not unexpected that ΔH_f contributes to E_V. The combination of the O 2p band center energy and E_g provides an estimate of the energy to transfer electrons left behind by the removed neutral O atom from the O 2p band into the newly created defect states that presumably reside within the gap. The actual combination of $(E_{O\,2p} + (1/2)E_g)$ results from treating these two quantities as separate terms, and strictly speaking, describes the energy transfer of electrons from the O 2p band center to the middle of the gap. In the context of accurately modeling E_V, the error in this approximation (the energy difference between the actual defect levels and the middle of the gap) is mitigated by the contributions of the other terms in eq 1. Finally, the $\langle\Delta\chi\rangle$ term adds a more explicit description of charge transfer between chemically bonded O and metal atoms. Large electronegativity differences correspond to highly ionic bonds with significant charge transfer from metal cations to O anions. V_O formation conversely involves transfer of O 2p electrons mainly to cation orbitals; therefore, large $\langle\Delta\chi\rangle$, and the consequent high intrinsic charge transfer from metals to O, increase the energetic resistance to the reverse transfer of V_O electrons from O to metals.

We also examine whether or not the use of accurate, but computationally expensive, GW gaps is necessary for the accuracy of our E_V model. Importantly, we do find that the less costly DFT+U gaps can substitute for GW values without significant loss of accuracy yielding a MAE of ~0.2 eV, as shown in Figure 1b. With this substitution, the E_V of the same 45 oxides from Figure 1a can be modeled by

$$E_V = 0.67\left[|\Delta H_f| + 0.60\left(E_{O\,2p} + \frac{1.5}{2}E_g^{DFT+U}\right) + 2.6\langle\Delta\chi\rangle\right] - 1.49 \quad (2)$$

Here, the DFT+U E_g prefactor of 1.5 originates from the slope of the best fit line for GW vs DFT+U gaps. Although we note that more sizable and nonsystematic inaccuracies in DFT+U gaps could result in additional outliers compared to E_V predictions from GW gaps, the results in Figure 1b indicate that the E_V of most compounds can be sufficiently well described by DFT+U E_g.

It is important to note that of the 45 oxides considered here, we have identified only one outlier, $HgTiO_3$. The inaccuracy of our model in predicting the E_V of $HgTiO_3$ arises from the inadequate treatment of the filled Hg d orbitals in DFT.[25] Application of a Hubbard U = 5 eV (instead of U = 0 eV) to the Hg d orbitals of $HgTiO_3$ results in a 30% decrease in the difference between the predicted and calculated E_V values. Overall, our model accurately describes the E_V values of ~98% of the 45 oxides with a MAE of ~0.2 eV.

The accurate prediction of E_V from DFT+U bulk material properties enables high throughput prediction of E_V. As a demonstration, and to validate the predictive power of our E_V model, we use our computational materials database (NRELMatDB)[14] to predict E_V for ~1800 stoichiometric and fully ordered oxides. We omit compounds with zero DFT+U gaps and compounds with O−O bonding (e.g., peroxides), because neither were included in the model development.

We validate the performance of our model against direct E_V calculations for a subset of 18 (1%) randomly chosen oxides

DOI: 10.1021/acs.jpclett.5b00710
J. Phys. Chem. Lett. 2015, 6, 1948−1953

not included in the original fitting set, including ternary and quaternary chemistries (Supporting Information Table S2). Comparison of the predicted and calculated E_V for this validation set, shown in Figure 1b inset, gives a MAE of 0.46 eV. The appearance of one outlier, K_3CoO_2, can be attributed to its unusual Co^{1+} oxidation state. Without K_3CoO_2, the MAE is 0.39 eV, indicating that our E_V model exhibits good overall predictive accuracy for a large range of chemistries. Individual differences between predicted and calculated E_V range from 0.0 to 0.9 eV. As already discussed, a portion of this error possibly arises from band gap inaccuracies inherent to DFT+U, and the performance of the model could be further improved with more accurate GW band gaps but at a significantly greater computational cost. Therefore, our E_V model describes ∼94% of the considered validation oxides with satisfactory overall accuracy.

Predicted E_V for ∼1800 oxides are shown in Figure 2 and grouped according to those containing (a) only main group metals, (b) TMs with zero spin (nonmagnetic), and (c) TMs with nonzero spin (magnetic). The results show that variations in E_V primarily result from the two most dominant contributions to the E_V model: ΔH_f and E_g. $E_{O\,2p}$ and $\langle\Delta\chi\rangle$ add additional variation such that materials exhibiting the lowest (highest) predicted E_V exhibit not only small (large) $|\Delta H_f|$ and E_g but also small (large) $E_{O\,2p}$ and $\langle\Delta\chi\rangle$, as supported by the physical insights discussed above. Consequently, materials with the lowest predicted E_V frequently contain late TMs (e.g., Au, Rh, Pt, Pd, Ir), whereas those with the highest predicted E_V commonly contain alkali, alkaline earth, or early TMs (e.g., Y, Hf, Zr) due to their respectively small and large $\langle\Delta\chi\rangle$. A complete list of the oxides and their properties is provided in Supporting Information Table S3.

Figure 2 suggests that nonmagnetic transition metal oxides (Figure 2b) exhibit the broadest range of material properties. These oxides exhibit a wide range of values for each term in the E_V model and, consequently, the predicted E_V range from ∼1−7 eV. In contrast, oxides containing magnetic TMs (Figure 2c) exhibit the most limited range of properties with predicted E_V ranging from ∼3−6 eV. Finally, oxides containing main group metals (Figure 2a) exhibit an intermediate range of properties. The variability across nonmagnetic TM oxides is well suited to applications requiring tunability of oxide properties. Nevertheless, the magnetic properties of some oxides provide additional functionality, and these oxides can be highly desirable for magnetic applications[26,27] where V_O secondarily affect material performance.

Predicted E_V provide a valuable metric to identify candidate materials for applications where V_O (or lack thereof) are of critical significance. For example, thermal-barrier coatings (TBCs) are widely used in gas turbine engines to enable high temperature operation by providing thermal insulation and oxidation resistance. Effective oxides for TBCs exhibit both high E_V to mitigate oxygen transport and good structural stability. We identify 31 unique compositions with predicted $E_V \geq 6.5$ eV (Supporting Information Table S3). Included in this set are ZrO_2 and Y_2O_3, the constituent oxides of the most commonly used TBC, yttria-stabilized zirconia. These 31 materials are also candidate refractories due to their high E_V and corresponding large $|\Delta H_f|$ which frequently results in good structural stability. Other commonly used refractories Al_2O_3, SiO_2, MgO, and CaO and numerous ternary and quaternary oxides are included in this set. We note that although E_V can be a critical selection criterion for a given application, most applications require materials to satisfy several metrics.

In conclusion, we have used first-principles calculations to elucidate the relationship between E_V and intrinsic material properties. Our results provide a direct and simple method to predict E_V at significantly reduced computational cost relative to direct calculations and offer valuable insights into the key properties that influence oxygen vacancy formation energetics, mainly the strength and character of chemical bonding and the effective electronic energy to transfer the oxygen vacancy electrons from the O 2p band into the defect levels. We predicted the E_V of ∼1800 oxide materials and discussed the results in the context of rapid material screening. We suggest this approach be extended to metallic oxides and charged defect states.

COMPUTATIONAL METHODS

Direct E_V Calculations. Our study focuses on the relationship between the intrinsic properties of oxides and the formation energetics of charge neutral oxygen vacancies. Standard supercell methods[11−13] were used to compute the E_V of a single, charge neutral V_O according to

$$E_V = E_{tot}^{defect} - E_{tot}^{host} + \mu_O \quad (3)$$

where E_{tot}^{defect} and E_{tot}^{host} are total energies of a supercell with and without the V_O, respectively, and μ_O corresponds to the oxygen chemical potential characterizing the reservoir of oxygen atoms. Supercells were generated by replicating DFT-relaxed bulk unit cells taken from the Inorganic Crystal Structure Database (ICSD)[28] and were constructed such that the distance between periodic V_O was ≥8 Å. Oxygen vacancies were created by removal of a neutral oxygen atom followed by self-consistent optimization of the electron density. In the language of Kröger−Vink notation, both the 2+ charged V_O and the charge compensating electrons are included in the supercell. Additional details are provided in the Supporting Information.

The computational approach adopted here and described in detail in the Supporting Information produces accurate defect energetics[11] as well as accurate ΔH_f.[29] Briefly, we performed spin polarized density functional theory (DFT+U)[30] calculations of E_V using the PBE exchange-correlation functional[31] and the projector augmented wave (PAW) method[32] as implemented in the VASP code.[33] A constant Hubbard term of $U = 3$ eV was applied to d orbitals of all transition metals except Cu and Ag, for which $U = 5$ eV was used, consistent with the numerical setup and findings from ref 29. We used fitted elemental reference energies (FERE),[29] which correspond to the standard state chemical potentials of the elements; therefore, our calculated E_V using the FERE oxygen chemical potential correspond to the standard state conditions of gaseous oxygen but can easily be adjusted for other T and P_{O_2} conditions.

Electronic Structure of the Host. To accurately model the electronic structure properties of the bulk (host) systems, in particular the E_g, spin-polarized many-body GW calculations with occupation independent on-site potentials for the 3d states of transition metals[25] were performed. Additional computational details are provided in the Supporting Information. E_g calculated using GW exhibit close agreement with experimental values, whereas E_g calculated using DFT+U generally underestimate experimental values (Figure 3), consistent with

DOI: 10.1021/acs.jpclett.5b00710
J. Phys. Chem. Lett. 2015, 6, 1948−1953

previous reports.[25,34,35] All gaps correspond to minimum (fundamental) gaps.

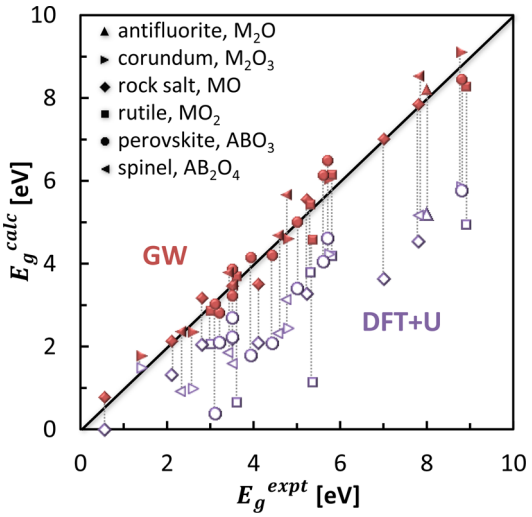

Figure 3. Calculated GW gaps (closed red symbols) exhibit close agreement with measured gaps while those from DFT+U (open purple symbols) significantly underestimate experimental values (E_g^{expt}).

Analysis Tools. A stepwise linear regression approach implemented in JMP[36] was used to investigate possible models for E_V and to select the most statistically significant subset of candidate descriptors using the corresponding p-values. The E_g and $E_{O\ 2p}$ descriptors were fit separately; however, linear regression produced a 1:2 ratio for these terms resulting in a combined descriptor given by the midgap energy relative to the O 2p band center ($E_{O\ 2p} + (1/2)E_g$). Additional information regarding the E_V model development is provided in the Supporting Information.

■ ASSOCIATED CONTENT

Supporting Information

Complete computational details, Figure S1 and S2, and tabulated values. The Supporting Information is available free of charge on the ACS Publications website at DOI: 10.1021/acs.jpclett.5b00710.

■ AUTHOR INFORMATION

Corresponding Author

*E-mail: vstevano@mines.edu.

Present Address

[‖](A.M.H.) National Renewable Energy Laboratory, Golden, Colorado 80401, United States.

Notes

The authors declare no competing financial interest.

■ ACKNOWLEDGMENTS

This research was supported by the National Science Foundation (NSF) under grant DMR-1309980. C.B.M. and A.M.H. acknowledge support from the NSF through grant CHE-1214131. Computational resources were sponsored by the Department of Energy's Office of Energy Efficiency and Renewable Energy and by the NSF (CNS-0821794) and the University of Colorado—Boulder.

■ REFERENCES

(1) Ginley, D.; Hosono, H.; Paine, D. C. *Handbook of Transparent Conductors*; Springer: New York, 2010.

(2) Adler, S. B. Factors Governing Oxygen Reduction in Solid Oxide Fuel Cell Cathodes. *Chem. Rev.* **2004**, *104*, 4791−4843.

(3) Kilner, J. A.; Burriel, M. Materials for Intermediate-Temperature Solid-Oxide Fuel Cells. *Annu. Rev. Mater. Res.* **2014**, *44*, 365−393.

(4) Chueh, W. C.; Falter, C.; Abbott, M.; Scipio, D.; Furler, P.; Haile, S. M.; Steinfeld, A. High-Flux Solar-Driven Thermochemical Dissociation of CO_2 and H_2O Using Nonstoichiometric Ceria. *Science* **2010**, *330*, 1797−1801.

(5) Muhich, C. L.; Evanko, B. W.; Weston, K. C.; Lichty, P.; Liang, X.; Martinek, J.; Musgrave, C. B.; Weimer, A. W. Efficient Generation of H_2 by Splitting Water with an Isothermal Redox Cycle. *Science* **2013**, *341*, 540−542.

(6) Mefford, J. T.; Hardin, W. G.; Dai, S.; Johnston, K. P.; Stevenson, K. J. Anion Charge Storage through Oxygen Intercalation in $LaMnO_3$ Perovskite Pseudocapacitor Electrodes. *Nat. Mater.* **2014**, *13*, 726−732.

(7) Fergus, J. W. Doping and Defect Association in Oxides for Use in Oxygen Sensors. *J. Mater. Sci.* **2003**, *38*, 4259−4270.

(8) Marcano, J. G. S.; Tsotsis, T. T. *Catalytic Membranes and Membrane Reactors*; Wiley: Weinheim, Germany, 2002.

(9) Padture, N. P.; Gell, M.; Jordan, E. H. Thermal Barrier Coatings for Gas-Turbine Engine Applications. *Science* **2002**, *296*, 280−285.

(10) Shackelford, J. F.; Doremus, R. H. *Ceramic and Glass Materials: Structure, Properties, and Processing*; Springer: New York, 2008.

(11) Lany, S.; Zunger, A. Assessment of Correction Methods for the Band-Gap Problem and for Finite-Size Effects in Supercell Defect Calculations: Case Studies for ZnO and GaAs. *Phys. Rev. B* **2008**, *78*, 235104.

(12) Freysoldt, C.; Neugebauer, J.; Van De Walle, C. G. Fully Ab Initio Finite-Size Corrections for Charged-Defect Supercell Calculations. *Phys. Rev. Lett.* **2009**, *102*, 1−4.

(13) Peng, H.; Scanlon, D. O.; Stevanović, V.; Vidal, J.; Watson, G. W.; Lany, S. Convergence of Density and Hybrid Functional Defect Calculations for Compound Semiconductors. *Phys. Rev. B* **2013**, *88*, 115201.

(14) NREL High Performance Computing Center Materials Database. http://materials.nrel.gov/ (accessed April 2015).

(15) Jain, A.; Ong, S. P.; Hautier, G.; Chen, W.; Richards, W. D.; Dacek, S.; Cholia, S.; Gunter, D.; Skinner, D.; Ceder, G.; et al. Commentary: The Materials Project: A Materials Genome Approach to Accelerating Materials Innovation. *APL Mater.* **2013**, *1*, 011002.

(16) Curtarolo, S.; Setyawan, W.; Hart, G. L. W.; Jahnatek, M.; Chepulskii, R. V.; Taylor, R. H.; Wang, S.; Xue, J.; Yang, K.; Levy, O.; et al. AFLOW: An Automatic Framework for High-Throughput Materials Discovery. *Comput. Mater. Sci.* **2012**, *58*, 218−226.

(17) Mizusaki, J.; Mima, Y.; Yamauchi, S.; Fueki, K.; Tagawa, H. Nonstoichiometry of the Perovskite-Type Oxides $La_{1-x}Sr_xCoO_{3-\delta}$. *J. Solid State Chem.* **1989**, *80*, 102−111.

(18) Bucher, E.; Sitte, W.; Caraman, G.; Cherepanov, V.; Aksenova, T.; Ananyev, M. Defect Equilibria and Partial Molar Properties of $(La,Sr)(Co,Fe)O_{3-\delta}$. *Solid State Ionics* **2006**, *177*, 3109−3115.

(19) Yamamoto, T.; Mizoguchi, T. First Principles Study on Oxygen Vacancy Formation in Rock Salt-Type Oxides MO (M: Mg, Ca, Sr and Ba). *Ceram. Interfaces* **2013**, *39*, S287−S292.

(20) Tanaka, I.; Tatsumi, K.; Nakano, M.; Adachi, H.; Oba, F. First-Principles Calculations of Anion Vacancies in Oxides and Nitrides. *J. Am. Ceram. Soc.* **2002**, *85*, 68−74.

(21) Murat, A.; Medvedeva, J. E. Composition-Dependent Oxygen Vacancy Formation in Multicomponent Wide-Band-Gap Oxides. *Phys. Rev. B* **2012**, *86*, 085123.

(22) Lee, Y.-L.; Kleis, J.; Rossmeisl, J.; Shao-Horn, Y.; Morgan, D. Prediction of Solid Oxide Fuel Cell Cathode Activity with First-Principles Descriptors. *Energy Environ. Sci.* **2011**, *4*, 3966−3970.

(23) Deml, A. M.; Stevanović, V.; Holder, A. M.; Sanders, M.; Musgrave, C. B.; O'Hayre, R. Tunable Oxygen Vacancy Formation

DOI: 10.1021/acs.jpclett.5b00710
J. Phys. Chem. Lett. 2015, 6, 1948−1953

Energetics in the Complex Perovskite Oxide $Sr_xLa_{1-x}Mn_yAl_{1-y}O_3$. *Chem. Mater.* **2014**, *26*, 6595−6602.
(24) Deml, A. M.; Stevanović, V.; Muhich, C. L.; Musgrave, C. B.; O'Hayre, R. Oxide Enthalpy of Formation and Band Gap Energy as Accurate Descriptors of Oxygen Vacancy Formation Energetics. *Energy Environ. Sci.* **2014**, *7*, 1996−2004.
(25) Lany, S. Band-Structure Calculations for the 3d Transition Metal Oxides in GW. *Phys. Rev. B* **2013**, *87*, 085112.
(26) Pan, Y.; Du, Z.; Zhao, F.; Xu, B. Magnetic Nanoparticles for the Manipulation of Proteins and Cells. *Chem. Soc. Rev.* **2012**, *41*, 2912−2942.
(27) Ren, Y.; Ma, Z.; Bruce, P. G. Ordered Mesoporous Metal Oxides: Synthesis and Applications. *Chem. Soc. Rev.* **2012**, *41*, 4909−4927.
(28) Belsky, A.; Hellenbrandt, M.; Karen, V. L.; Luksch, P. New Developments in the Inorganic Crystal Structure Database (ICSD): Accessibility in Support of Materials Research and Design. *Acta Crystallogr., Sect. B: Struct. Sci.* **2002**, *B58*, 364−369.
(29) Stevanović, V.; Lany, S.; Zhang, X.; Zunger, A. Correcting Density Functional Theory for Accurate Predictions of Compound Enthalpies of Formation: Fitted Elemental-Phase Reference Energies. *Phys. Rev. B* **2012**, *85*, 115104.
(30) Dudarev, S. L.; Botton, G. A.; Savrasov, S. Y.; Humphreys, C. J.; Sutton, A. P. Electron-Energy-Loss Spectra and the Structural Stability of Nickel Oxide: An LSDA+U Study. *Phys. Rev. B* **1998**, *57*, 1505−1509.
(31) Perdew, J. P.; Burke, K.; Ernzerhof, M. Generalized Gradient Approximation Made Simple. *Phys. Rev. Lett.* **1996**, *77*, 3865−3868.
(32) Blöchl, P. Projector Augmented-Wave Method. *Phys. Rev. B* **1994**, *50*, 17953−17979.
(33) Kresse, G.; Furthmüller, J. Efficiency of Ab-Initio Total Energy Calculations for Metals and Semiconductors Using a Plane-Wave Basis Set. *Comput. Mater. Sci.* **1996**, *6*, 15−50.
(34) van Schilfgaarde, M.; Kotani, T.; Faleev, S. Quasiparticle Self-Consistent GW Theory. *Phys. Rev. Lett.* **2006**, *96*, 226402.
(35) Shishkin, M.; Kresse, G. Self-Consistent GW Calculations for Semiconductors and Insulators. *Phys. Rev. B* **2007**, *75*, 235102.
(36) *JMP Pro*, Version 11; SAS Institute Inc.: Cary, NC, 2014.

DOI: 10.1021/acs.jpclett.5b00710
J. Phys. Chem. Lett. 2015, 6, 1948−1953